MSc in Photonics
Universitat Politècnica de Catalunya (UPC)
Universitat Autònoma de Barcelona (UAB)
Universitat de Barcelona (UB)
Institut de Ciències Fotòniques (ICFO)

http://www.photonicsbcn.eu

PHOTONICS**BCN**

Master in Photonics

MASTER THESIS WORK

Nanoscale control of heat generation with plasmonic nanostructures

Jordi Morales Dalmau

Supervised by Prof. Romain Quidant, (ICFO)

Presented on date 19th July 2013

Registered at

Escola Tècnica Superior d'Enginyeria de Telecomunicació de Barcelona

Nanoscale control of heat generation with plasmonic nanostructures

Jordi Morales Dalmau
ICFO, Plasmon Nano-Optics Group, Mediterranean Technology Park Av. Carl Friedrich Gauss, 3 08860 Castelldefels (Barcelona), Spain

E-mail: Jordi.morales@icfo.es

Keywords: Plasmonics, heat, thermal-lens, temperature.

Abstract. During the last 25 years, a huge effort has been devoted to understand and exploit the novel properties arising from the size reduction of matter to the nanoscale. Nanotechnologies are now used in fields ranging from physics and chemistry to biology and medicine. In this context, we have developed new tunable thermal lenses based on plasmonic structures. To demonstrate and describe the thermal lensing effect we combine numerical simulations with optical measurements. We first simulate the change of refractive index of water produced by a microdisc heated to different temperatures. Based on these simulations, we fabricate and characterize the resulting thermal lens. Our experimental data show that a 10 μm plasmonic nanorods (NR) array optically excited at local plasmonic resonance (LPR) in contact with water acts as a divergent lens of 13 μm size. When combined with a convergent lens, the ensemble acts as a convergent lens whose focal distance is tunned by heating the plasmonic nanostructures.

1. Introduction

Over the last 20-30 years, nanotechnology has become a very rich transversal science with key implications on Physics, Chemistry, Biology or Medicine[1]. Richard Feynman understood already in the 60's that nanotechnology had the capability to manipulate systems on a molecular level [2].

Nanotechnology is based on the size reduction of materials down to the nanoscale. When reducing the size, the surface to volume ratio increases which leads to new physical properties. For example, the number of atom present on the surface of a 10 nm gold sphere is higher compared to the number inside the nanoparticle (NP). Also, the size reduction implies a confinement inside the object. Its behaviour then strongly depends on the size and shape of the NP. In other words, the particle - electrons or phonons for example- are strongly affected by the boundary conditions of the system. This confinement can be a quantum confinement like in quantum dots, or could be a dielectric confinement leading to the existence of surface plasmons in metallic NP. By taking advantage of this dependence, it is possible to tune the physical properties of an object by modifying its shape or size. These phenomena explain the huge potential associated to nanotechnologies as well as their challenges since it is necessary to control the shape and size at the nanoscale[3].

Metallic structures coupled with electromagnetic radiation are usually described by a free oscillation of the conduction electrons inside the metal. The field that describes interaction of light with metallic NPs is known as *plasmonics*[2]. A plasmon is considered as a collective electron oscillation inside a metallic NP. The resonance of this oscillation occurs in the visible-NIR range when consider gold or silver NPs[4]. The position of the resonance can be tuned by changing the shape or size of the NP which acts as a cavity. Thus, non-isotropic NPs present several resonances associated to the different dimensions. For instance, spherical gold NPs support a resonance in the green region whereas nanorods feature a resonance that can be shifted in the NIR region and depends on its aspect ratio. The surface plasmon resonance (SPR) associated to collective oscillation of the electrons leads to two effects. Firstly, a NP scatters efficiently light because of the strong oscillating dipole associated to the collective oscillation. Secondly, a NP absorbs a part of this light because of oscillation damping[5] (electron-electron collisions) and then behaves as a heat[6] nanosource. This photo-induced heating leads to a temperature increase around the particle. This effect can be used for different applications in optofluidics[7] and in biology for example[8]. The emission and the absorption of light by a NP can be controlled by modifying its shape or geometry[9].

In this work, we focus on the heat generation induced by the absorption of light by plasmonic structures. The heat released by the structures increases locally the temperature at their vicinity. This temperature change induces an optical index profile inside the environment of the structures, which acts as a lens. Here I show how a proper engineering of the thermal profile near plasmonic nanostructures can be exploited to create an optical microlens whose focal length can be tuned by a control laser.

2. Lensing effect

2.1. Ability to generate heat: Nanostructures

Plasmonic structures generate heat absorbing light. That effect can be enhanced by using a wavelength matching at the plasmonic resonance. During this work, we show a complete study of the temperature profile both by experimentally measuring the temperature[10,11] and theoretically by performing finite element simulations of disc-like plasmonic structures.

2.1.1. Sample

Two different micrometric samples have been developed. The first sample (figure 1a) is a 10 µm homogeneous gold disc. The second one (figure 1b) is a 10 µm diameter disc formed of gold nanorods (NRs). In this case, we have worked with different separation (pitch) between NRs, and different aspect ratio of NRs in order to tune the SPR at 840 nm for our experiments.

NRs are illuminated at their longitudinal surface plasmon resonance (LSPR) to maximize heat generation. In this case, we have worked at a fixed wavelength λ=840nm using a Ti:Saphire laser in continuous mode that corresponds to their resonance when the incident electric field is polarized along the main antenna axis, as shown in the insert of figure 1b. To get a plasmonic structure resonant at 840nm, several aspect ratio antennas have been designed. We found that 120x80x50nm were resonant at that wavelength, whereas a shift of 40 nm was found for 140x80x50nm antenna, for example. This shows the sensitivity of SPR with respect to the aspect ratio. Also the pitch -distance between antennas- has been tuned to maximize the amplitude of the absorption without modifying the spectral position of the resonance because of the electromagnetic coupling between antennas. In this case a 300 nm pitch has been chosen. To analyse the resonance effect, we compare a parallel resonant configuration with a cross polarized off resonant one.

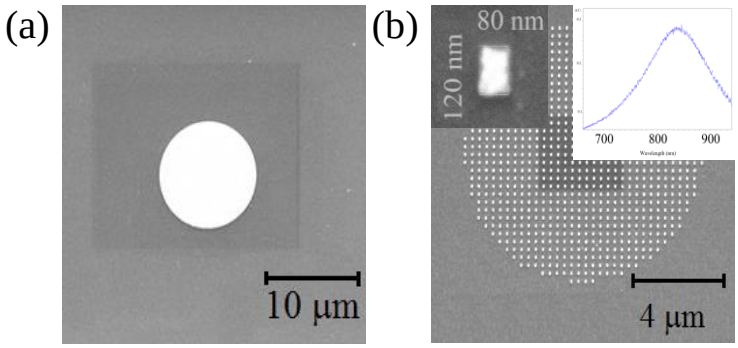

Figure 1. Scanning Electron Microscopy (SEM) images of lithographic samples. Gold disc of 10 µm diameter (a) and made of 120x80x50 gold NRs with a pitch of 300 nm (b). Inserts of figure 1b are zoom of a gold NR (top-left) and spectral response of the structure (top-right).

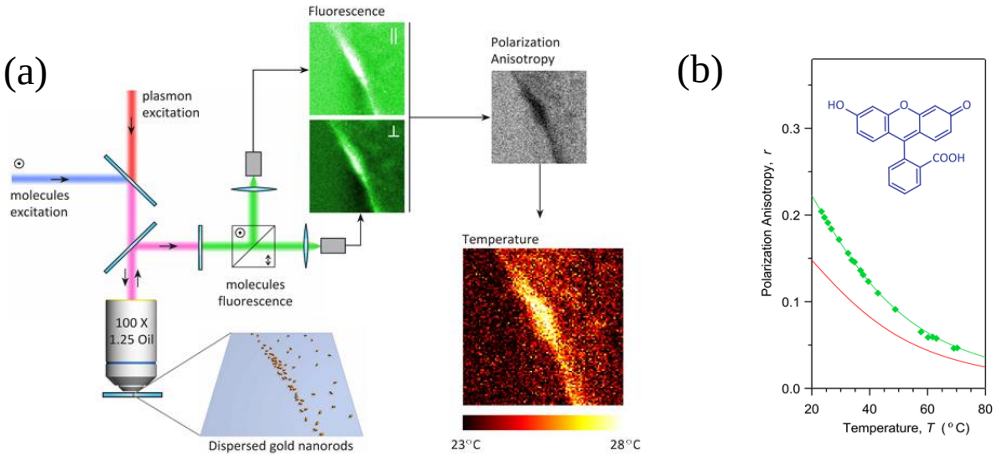

Figure 2. (a) Scheme of set-up for nanoscale temperature measurement using anisotropy values of the medium and (b) fluorescence polarization anisotropy calibration. Theoretical curve (solid green line) of fluorescence polarization anisotropy as a function of the temperature for fluorescine dissolved in a glycerol-water (4:1) mixture. Taken from [10].

2.1.2. Thermal microscopy

To measure the temperature at the nanoscale, we use a well-established set-up with recently published papers[10,11]. Fig 2a presents the principle of the technique where two laser beams are used: a red laser heats the sample and a blue laser –probe beam- excites fluorescence of fluorescine. The detection of the setup uses a beam splitter to divide the signal on two amplifying photo detectors (APDs) and then to be able to register separately the intensity of fluorescence for each polarization named $I_{\parallel}$ and $I_{\perp}$. The final anisotropy *r* is obtained with these two intensities using eq. (1)[10]. To link anisotropy and temperature we perform a calibration curve using fluorescent sample and a thermostat (figure 2b). Thanks to this calibration this technique enables to measure temperature in a non-invasive fashion by measuring fluorescence anisotropy.

$$r = \frac{I_{\parallel} - I_{\perp}}{I_{\parallel} + 2I_{\perp}} \qquad (1)$$

2.1.3. Temperature measurements

We have measured the temperature of our different discs immersed in a mixture of water and fluorescine for different heating powers using the setup described above. In figure 3a, the power dependence of temperature for different structures and polarizations when an 840nm red laser excites the plasmonic structure is shown. The NR disc generates the highest temperature increase for all powers and, because of the plasmonic behaviour, when cross polarization is shined on NR structures, the temperature variations decreases by a factor 2. As the raise of temperature is linear with the incoming power of the laser for all structures[10], the different heat abilities of the considered samples are given by the slope of the curves. The higher the slope of temperature in function of power is, the more efficient the system is producing heat. To highlight the structure dependence of the temperature, we show the map of the temperature recorded on the different configurations under a 20mW 840nm laser exciting the sample.

Finally, we show in figure 3b the temperature profile at different heights for a 120x80x50 NR disc with a heating power of P=20mW. As expected for a diffusive process, we observe a drop of the temperature while increasing the height of the observation plane.

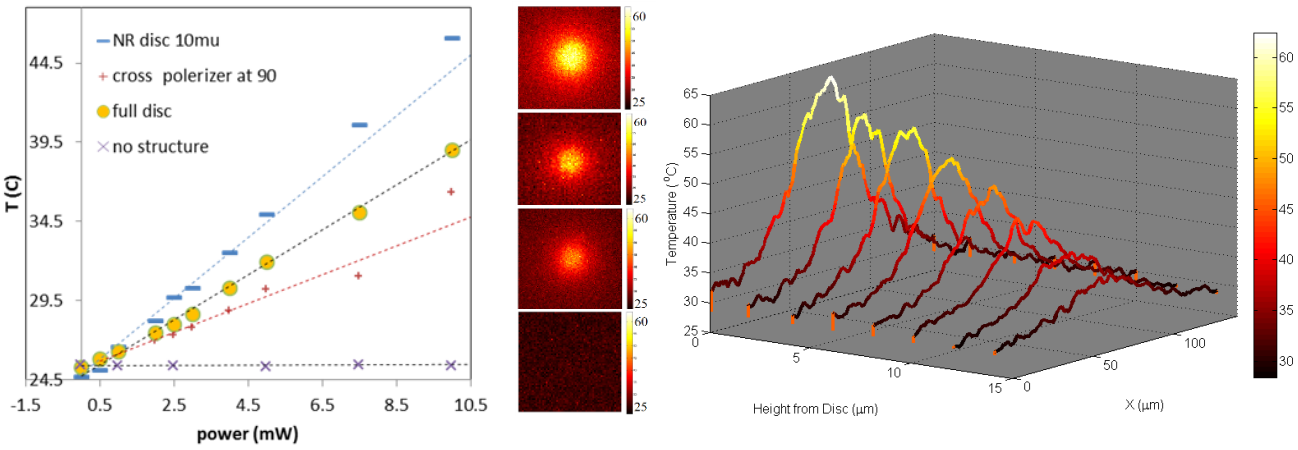

(a) (b)

Figure 3. Temperature map as function of heating power: 10 µm disc made of NRs with parallel (red dot) and crossed polarization (black dot); 10 µm gold disc (blue cross) and no structure (magenta star) (a). Images of the temperature measured with the setup at P=20mW, right (a). Temperature distribution of a cross-cut of 120x80x50 NR disc for different heights at same heating power (b).

2.2. Dependence of the refractive index with temperature

Refractive index of material depends on several parameters such as wavelength –called dispersion-, temperature, pressure… For example, this effect has been used to obtain more efficient and tunable waveguides[12] in the context of information processing. In this project, we want to induce a change in the refractive index of a liquid to create a lens. By taking advantage of the ability of gold disc-like structures to generate a temperature increase (figure 3), it is possible to change the optical index of water in the vicinity of these structures when they are excited with a laser. We can use the literature to obtain an expansion of the influence of the temperature and wavelength in the refractive index of different liquids[13,14,15]. Figure 4 displays the dispersion and temperature dependence of the optical index of water [13]. In this case, when the temperature rises, the optical index of water decreases. This change on the refractive index creates a negative phase accumulation which can be physically associated to a divergent lens effect.

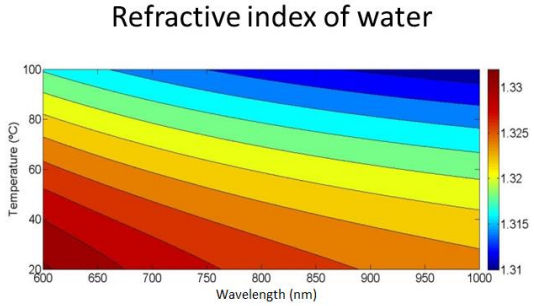

Figure 4. Refractive index of water as a function of the incoming wavelength and temperature of the medium. The relationship for water is from literature [13].

2.2.1. Theoretical simulations of the lensing effect

To understand and analyse such thermo lensing effect, we have performed simulations. First, we have calculated the temperature distribution induced inside water by a hot disc deposited on glass using COMSOL®. Figure 5a shows the temperature profile induced by a 10 µm disc of gold sailed at 73ºC positioned inside a 100x50 μm^2 box of water. Then, using the temperature dependence of the optical index of water[13], we have calculated the optical index profile shown in figure 5b. The temperature distribution creates a negative gradient of water's refractive index. By integrating the optical index variation over the z-direction, we obtain the shape of the thermal lens induced inside the water by the heated gold disc (figure 5c) with a circular symmetry centred at the disc. To interpret this optical index variation as a lens, we will use the classical thin lens approximation because the variation occurs on a size mush large than the wavelength -10µm gold disc-. In this case, the power of the lens associated to an optical index variation is given by the lens maker equation (2).

$$\mathrm{P} = \frac{1}{\mathrm{f}} = \Delta\mathrm{n}\left[\frac{1}{\mathrm{R}_1} - \frac{1}{\mathrm{R}_2} + \frac{\Delta\mathrm{nd}}{\mathrm{nR}_1\mathrm{R}_2}\right] \quad (2)$$

where P is the power, f is the focal distance, d is the thickness and Δn is the refractive index variation. In our case R_1 is infinite –planar surface- and R_2 is estimated by the full width half maximum (FWHM) of the in-plane optical index profile. Using this model we have calculated the focal distance for each height of water, which depends on the in-plane variation of refractive index. We observe that the focal distance increases strongly toward infinity –no lensing effect- while increasing the distance with respect to the heating plasmonic structure. Finally, we describe this complex configuration by a simple divergent lens (figure 6). To do so, we first integrate the power of the lenses associated to each height. On figure 6a, this effective focal distance $\frac{1}{f_{eff}} = \int_0^z \frac{1}{f(z\prime)} dz'$ is given as a function of z. We observe a convergence toward -400µm when z is closed to 2µm. This shows that the lensing effect is obtained within the first microns. This result allows us to describe a 73 degree Celsius disc immersed in water as a thermal lens of -400µm focal distance lens, with a thickness of few microns and an in-plane size of 20µm (FWHM of optical lens profile (figure 5c)). Moreover, this study is completed by computing the effective focal distance for different temperatures with discs with same 5µm size (figure 6b) and different size of the discs at the same temperature (figure 6c). We observe an asymptotic behaviour of the effective focal distance while increasing the size of the disc (figure 6c). So, by increasing the radius of the disc more than about 5µm, results are not going to change substantially. For smaller radius, we observe a decrease of the effectiveness of the lens. This can originate from the diffusivity of temperature that spreads over few microns for each punctual source. On the other hand, by changing the temperature of the structure and then the effective refractive index of water (figure 6d), the effective focal distances is progressively tuned. This result validates the assumption of obtaining a tunable thermal lens by changing the temperature of the source when considering a fixed 5µm radius gold disc for which the lensing effect is close to saturation.

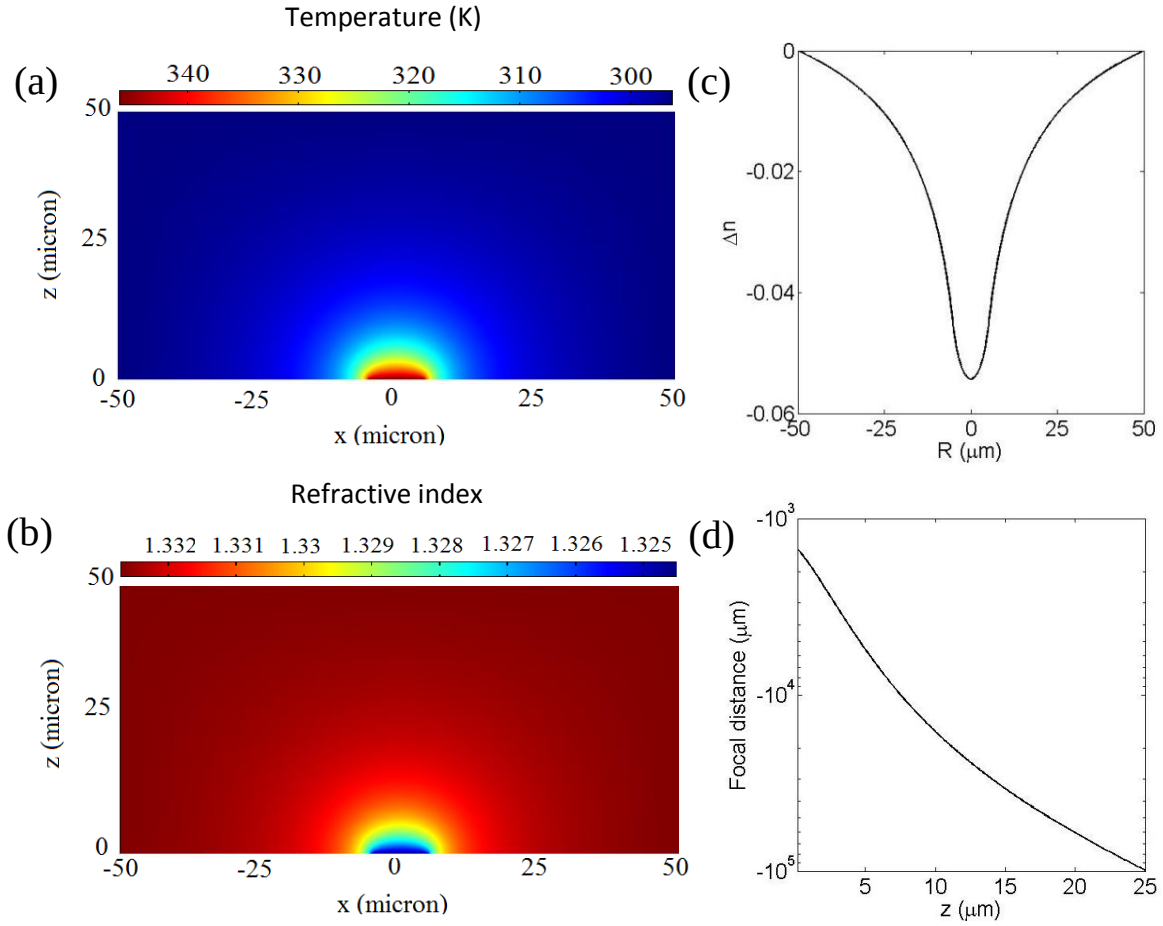

Figure 5. Simulations of thermal lens effect. (a) Map of the temperature simulated in Comsol® of a 10 μm diameter gold disc in a 100x50 μm^2 box of water; (b) Map of the optical index using Taylor expansion for temperature; (c) Cross-cut of the optical index along XY plane and (d) focal distance of different Z plane using thin lens approximation (2).

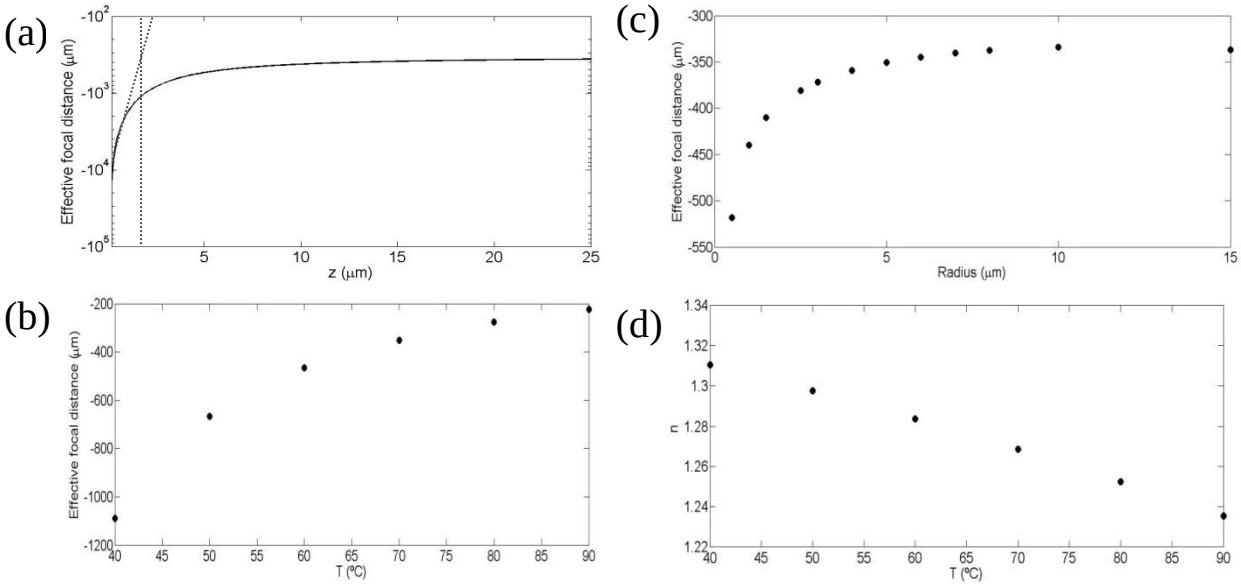

Figure 6. Characterization of thermal lens effect. (a) Accumulative effective focal distance for different z planes; (b) Effective focal distance for different temperatures for 10 μm diameter gold disc; (c) Effective focal distance for different radius gold disc at 73ºC and (d) effective refractive index for 10 μm diameter gold disc at different temperatures.

2.2.2. Experimental measurement of the lensing effect

The experimental systems we use are different gold discs of 10 µm diameter made of NRs, immersed in water that contains green fluorescent protein (GFP) (figure 7a). We perform two experiments. First we record the fluorescence from the GFP for different heights without the heating laser –red beam on figure 7a-, by changing the position of the sample with a piezoelectric stage. In a second time, we measure the fluorescence map in presence of the heating laser. We generate a shift of the focus of the probe beam by increasing the power of the heating beam. To measure both fluorescence intensity from a sample and characterize the shift of the focus, we use a confocal system. The blue beam, which excites the fluorescence and is going to be defocused, is shined from the bottom with a microscope objective lens of 50X. The excited fluorescence is registered by an APD.

First, we achieve the calibration of the fluorescence as function of height. Because the fluorescence signal is collected from the fixed focal plane of the objective –without thermal lens-, we obtain different intensities depending on the height where we measure (figure 7b). Then, a red laser resonant with the plasmonic structure is shined onto the sample –as described in figure 7a- in order to increase the temperature and induce the lensing effect. In this case, we measure the fluorescence from the centre of the sample at a fixed height. The position of the focus starts below the centre of the fluorescine sample, and while increasing the heating power, the focus is shifted to the centre of the sample, which gives the highest value of the fluorescence signal. When increasing the power even more, the focus is shifted after the centre of the sample as we can see in figure 7b. Because of the divergence nature of the lens, the focal plane of the probe beam changes from bottom to top of the fluorescine when increasing the power from 0 to 30mW.

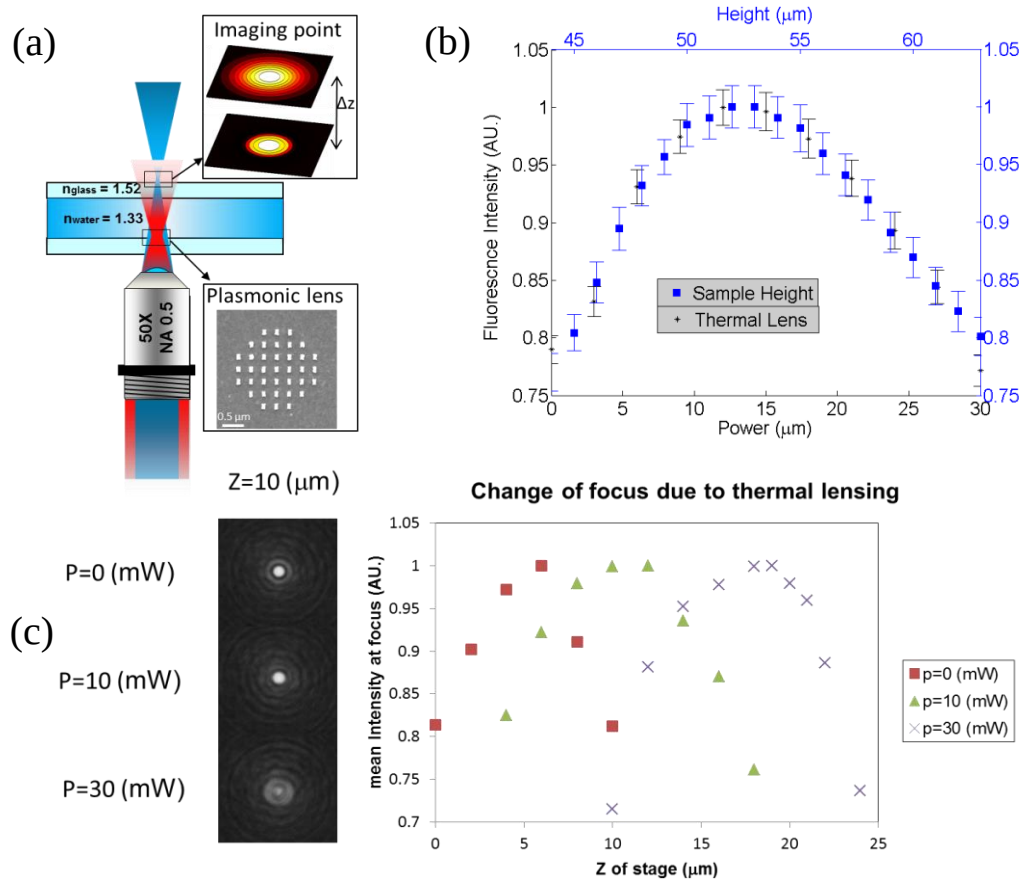

Figure 7. (a) Scheme of the setup to measure the fluorescence fluctuation; (b) Normalized fluorescence intensity for different z planes, top x-axis (blue) and changed by thermal lens effect, bottom x-axis (red) and (c) width at different z-planes of the probe beam for different powers.

To go further, we have measured the intensity of the blue beam as a function of the stage height in absence and in presence of heating laser –figure 7c-. In both cases, we observe a maximum of the intensity associated to the focal point. The shift of the maximum position originates, from the lensing effect as we observe, a shift of the focal point of 5µm and 15µm when 10mW and 30mW were applied, respectively. This shows that the sensibility of the lens is close to 0.5µm/mW. Considering the stability of the Ti:Sapphire laser –stability power of <0.25% rms-, this means that accuracy of thermal lens can be estimated to 2.5nm/mW.

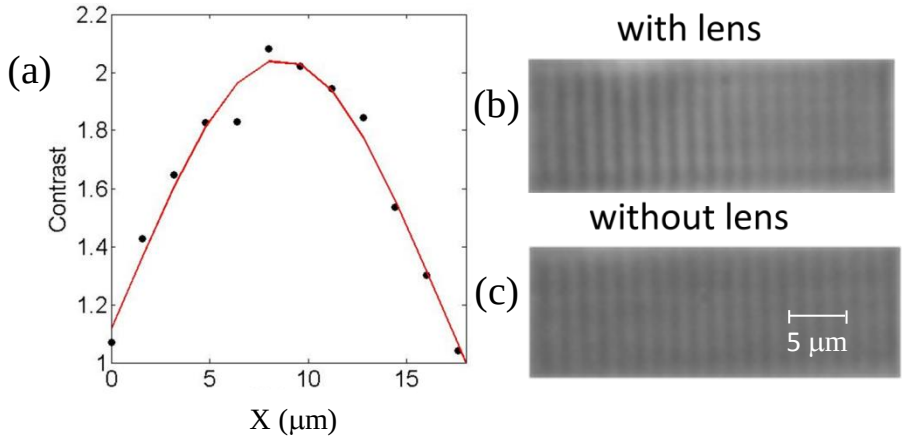

Figure 8. Change of contrast of a ruler made of lines with a separation of 1.4 µm with and without thermal lens effect.

To characterize the in-plane size of the generated thermal lens as well as analyse its performance, we have taken an image of a ruler in absence of thermal lens when the ruler is out of focus and after switching of the thermal lens that focus the ruler. We have then measured the contrast of each line of the grating in both cases. Figure 9 represents the ratio of the contrast. We see that the presence of the thermal lens enables to increase the contrast by a factor 2. The size of the lensing effect can be attributed to FWHM of the contrast curve and has been evaluated to 13µm in this case.

To show the applicability of a thermal lens in biological samples the focus of a cells single layer is changed (figure 9). Thermal effect is achieved on the image while changing the power of the red laser, from 0mW (a) to 40mW (b). We obtain a difference in contrast due to the defocusing where the last image seems to be more focused on the cell than first one.

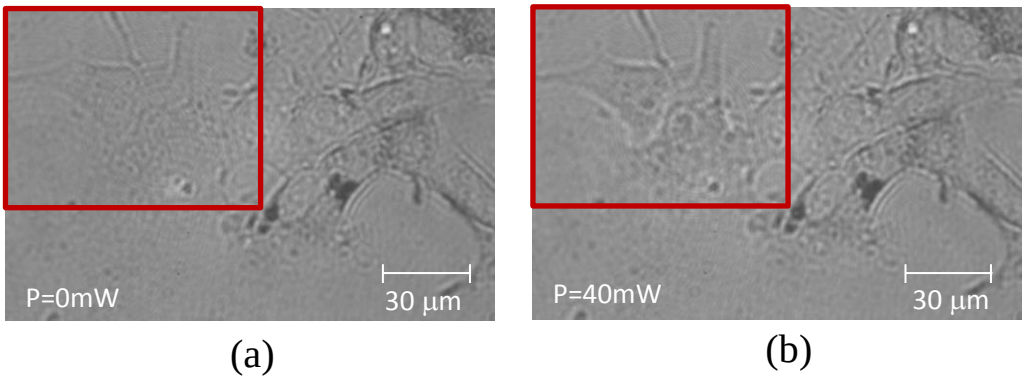

Figure 9. Local thermal lensing effect on biological sample. Defocused and focused cell on of the image (red square). Heat laser at P=0mW (a) and at P=40mW (b).

3. Conclusions

By taking advantage of the temperature dependence of the optical index of materials, and water in particular, together with the ability of plasmonic structure to generate heat efficiently, we have developed a thermal lens based on plasmonic structure heating. First, the effect has been analysed by performing numerical simulations. Then, an experimental demonstration has been realized. The nice results emanating from these primary experiments are promising and demonstrate the potential of this idea. Such a tunable and cheap lens concept can be useful in different areas and we here show its application on a biological sample.

Acknowledgments

I thank ICFO, Prof. Lluis Torner and Prof. Romain Quidant for welcoming me in this project and bringing to me the opportunity to develop my scientific skills and knowledge. Particularly, I want to mention Plasmonic Nano-Optics Group and Prof. Romain Quidant for his guidance and encouragement. Also I thank Jon Doner and Dr. Renaud Marty for cooperation and help through various stages.

References

1. Bhattacharyya, D., Singh, S. & Satnalika, N. Nanotechnology , Big things from a Tiny World : a Review. *International Journal of u- and e- Service, Science and Technology* **2**, 29–38 (2009).

2. Hayashi, S. & Okamoto, T. Plasmonics: visit the past to know the future. *Journal of Physics D: Applied Physics* **45**, 433001 (2012).

3. Novotny, L. & Hecht, B. *Principles of Nano-Optics*. (Cambridge: 2006).

4. Jain, P. K., Huang, X., El-Sayed, I. H. & El-Sayed, M. a. Review of Some Interesting Surface Plasmon Resonance-enhanced Properties of Noble Metal Nanoparticles and Their Applications to Biosystems. *Plasmonics* **2**, 107–118 (2007).

5. Bosman, M. *et al.* Surface plasmon damping quantified with an electron nanoprobe. *Scientific reports* **3**, 1312 (2013).

6. Baffou, G. & Quidant, R. Thermo-plasmonics: using metallic nanostructures as nano-sources of heat. *Laser & Photonics Reviews* **7**, 171–187 (2013).

7. Donner, J. S., Baffou, G., McCloskey, D. & Quidant, R. Plasmon-assisted optofluidics. *ACS nano* **5**, 5457–62 (2011).

8. Huang, X., El-Sayed, I. H., Qian, W. & El-Sayed, M. a Cancer cell imaging and photothermal therapy in the near-infrared region by using gold nanorods. *Journal of the American Chemical Society* **128**, 2115–20 (2006).

9. Baffou, G., Quidant, R. & Girard, C. Heat generation in plasmonic nanostructures: Influence of morphology. *Applied Physics Letters* **94**, 153109 (2009).

10. Baffou, G., Kreuzer, M. P., Kulzer, F. & Quidant, R. Temperature mapping near plasmonic nanostructures using fluorescence polarization anisotropy. *Optics express* **17**, 3291–8 (2009).

11. Donner, J. S., Thompson, S. a, Kreuzer, M. P., Baffou, G. & Quidant, R. Mapping intracellular temperature using green fluorescent protein. *Nano letters* **12**, 2107–11 (2012).

12. Tang, S. K. Y., Mayers, B. T., Vezenov, D. V. & Whitesides, G. M. Optical waveguiding using thermal gradients across homogeneous liquids in microfluidic channels. *Applied Physics Letters* **88**, 061112 (2006).

13. N Bashkatov, Alexey and A Genina, E. Water refractive index in dependence on temperature and wavelength: a simple approximation. *Optical Technologies in Biophotonics and Medicine IV. SPIE* **5068**, (2003).

14. Beysens, D. & Calmettes, P. Temperature dependence of the refractive indices of liquids: Deviation from the Lorentz–Lorenz formula. *The Journal of Chemical Physics* **66**, 766 (1977).

15. Franko, M. & Tran, C. D. Water as a unique medium for thermal lens measurements. *Analytical Chemistry* **61**, 1660–1666 (1989).